Supporting Information

Chhabra et al. 10.1073/pnas.1118680109

SI Methods

Cloning, Expression, and Purification of Proteins. TR_{NRP} and R_{NRP} were cloned from 5,968 bp and 6,166 bp to C terminus of *Mycobacterium tuberculosis* (*M. tuberculosis*) gene Nrp, respectively. TR_{GPL} and R_{GPL} were cloned from 6,103 bp and 6,301 bp to C terminus of *Mycrobacterium smegmatis* gene *mps2*, respectively. All primers were engineered with suitable restriction sites to facilitate cloning in *Escherichia coli* (*E. coli*) expression vectors pET 28c or pET 21c (Novagen). The R_{GPL} mutants were constructed in accordance with the manufacturer's protocol using QuickChange site-directed mutagenesis kit XL (Stratagene), mutagenic primers (Table S2), and confirmed by automated DNA sequencing. All proteins were expressed in BL21-DE3 strain of *E.coli* in the soluble fraction by inducing cultures at low temperatures and isopropyl β-D-thiogalactopyranoside concentrations. Rv0100 was expressed in BL21-DE3 strain coexpressing Sfp protein of *Bacillus subtilis*. Selenomethionine-derivatized R_{NRP} protein was purified from BL 834 auxotroph strain of *E.coli*. The proteins were purified to homogeneity by Ni^{+2}-NTA affinity chromatography owing to their N- or C-terminal hexa-Histidine tag. Further purification for crystallization was performed by gel filtration using Superdex 200 GF column preequilibrated with 20 mM NaCl, 20 mM Tris-Cl, pH-8.0 and 5 mM dithiothreitol (DTT).

Enzymatic Assays. The peptidyl-CoA conjugate was prepared by the reaction of 4.0 eq coenzyme A sodium salt (Sigma-Aldrich) with peptide (1.0 eq), 4.0 eq of benzotriazol-1-yl-oxytripyrrolidinophosphonium hexafluorophosphate or pyBOP (Novabiochem), and 4.0 eq of potassium carbonate in 1 : 1 tetrahydrofuran/water mixture. The reaction mixture was stirred at room temperature for 6 h, frozen in liquid nitrogen, and lyophilized. After diethyl ether washes the peptidyl-CoA was purified on C18 RP-HPLC column using a gradient of 0–60% B in 25 min (A-water with 0.1% TFA and B-Acetonitrile with 0.1% TFA) and the identity of the conjugate was confirmed by mass spectrometry. Boc-alanine and Boc-phenylalanine were conjugated to coenzyme A using N,N′-dicyclohexylcarbodiimide/1-Hydroxybenzotriazole (DCC/HOBt) coupling and purified similarly on HPLC. The aldehyde valeryl-*L*-Phe-*L*-Thr-*L*-Ala-*L*-Alaninal (valeryl-FTAA-laninal) was synthesized by Fmoc solid phase chemistry using the Weinreb AM resin (Novabiochem, 0.63 mM/g) and automated peptide synthesizer (Advanced Chemtech, USA). Cleavage of the peptide aldehyde from the resin was performed by adding lithium aluminum hydride (Aldrich, 2 M). The reaction was quenched with careful addition of $KHSO_4$ (saturated solution). The aldehyde could be purified from other impurities (including traces of alcohol, valeryl-FTAAlaninol) on C18 RP-HPLC column (7.8 × 300 mm, 125 Å, Waters) using a gradient of 0–48% B in 20 min, 48% B in 40 min, and 90%B in 50 min (A: water with 0.1% TFA and B: acetonitrile with 0.1% TFA), and identity was confirmed by ESI-MS analysis.

Purified R_{GPL}/R_{NRP} 5–120 μM, valeryl-FTAA-CoA 200 μM, and NADPH 2 mM were incubated at 30 °C for 2 h. The protein was precipitated with acetonitrile, and the reaction mix was loaded on C18 RP-HPLC column on a gradient of 5 to 48% B in 25 min, 48% B in 40 min, and 70%B in 50 min (A-water with 0.1%TFA and B-acetonitrile with 0.1%TFA) after incubation at 30 °C for 2 h. The identity of peak was confirmed by TOF-MS and tandem mass spectrometric analysis using ESI-MS (API QSTAR Pulsar i MS/MS, Applied Biosystems). For kinetic analysis, the reaction was set up using 5–50 μM protein, 0.5–5 mM substrate, and 0.2 mM NADPH and the change in NADPH absorption at 340 nm was monitored spectrophotometrically (Varian). Cell-free reconstitution assays with fatty acyl-CoAs were set up using a total of 100 μM fatty acyl-CoA or aldehyde (inclusive of 5–30 μM of [1-^{14}C] fatty acyl-CoA (55 mCi/mmole, American Radiolabeled Chemicals (ARC) or [1-^{14}C] lauraldehyde, respectively), 2 mM NADPH and 5–50 μM protein for 1–2 h. A [1-^{14}C] lauroyl aldehyde was obtained enzymatically from [1-^{14}C] lauric acid (55 mCi/mmole, ARC) using recombinant *M. tuberculosis* fatty acyl-activating enzyme FadD9. The products were extracted twice in 300 μL of hexanes, resolved on silica gel 60 F_{254} TLC plates (Merck) using 80 : 20 hexanes : ethyl acetate (*vol*/*vol*) solvent system, detected and quantitated using Phosphor imager (Fuji BAS500) by comparing Rf to synthetic standards (Sigma and ARC). Fatty acid activation by FAAL10 and transfer onto Rv0100 was analyzed using enzyme assays described previously (1).

Crystallization, Data Processing, and Refinement of R_{NRP}. Initial crystallization conditions obtained from crystal screens 1 and 2 (Hampton Research) were modified, with final reservoir solution containing 2.5 M ammonium sulfate, 100 mM MES at pH 7 resulting in large and well-diffracting crystals. A single wavelength anomalous dispersion (SAD) dataset was collected to a resolution of 2.3 Å (λ : 0.97 Å) at X-12 beamline at European Molecular Biology Laboratory, Hamburg, Germany, at 100 K. While collecting the data at beamline, its quality and redundancy were assessed using AUTORICKSHAW (2) in order to ensure sufficient redundancy for structure determination by SAD phasing. The diffraction data was indexed and integrated with HKL2000 (3) in space group $P3_121$ with cell dimensions of $a = b = 59.06$, $c = 239$, $\alpha = \beta = 90°$, $\gamma = 120°$. The solvent content was estimated to be 46.8%, and it has one monomer per asymmetric unit. The initial phasing was done using AUTOSOL of PHENIX (4). This procedure located all the eight heavy-atom sites (overall FOM = 0.3). Initial model was built using AUTOBUILD from PHENIX, which was improved using O (5) and COOT (6). Structure refinement was done using CNS (7) with final round of refinement with translation/libration/screw mode in REFMAC5 (8) resulting in final R_{work}/R_{free} of 22.94/27.77. We have used default parameters while refining the structure either in CNS or REFMAC5. Using PROCHECK (9); 89.3% of the residues were found to be in most favored regions and 10.4% residues in additionally allowed regions and 0.3% residues in generously allowed region. Waters were included using O program and were edited using 2*Fo-Fc* and *Fo-Fc* map using the program O. Figures representing the crystal structure were prepared using PyMol (The PyMOL Molecular Graphics System, Version 1.2r3pre, Schrödinger, LLC).

Structural Modeling and Small Angle X-Ray Scattering (SAXS) Studies. The valeryl-FTAA-ppant was modeled into the C-terminal domain of R_{NRP} based on PDBID:1W6U. Model of Nrp termination module based on 2VSQ (sequence identity 30%) helped in placement of ppant arm of the substrate. R_{NRP} crystal structure was used as template for R_{GPL} model. Both models were generated using MODELLER (10). SAXS analysis: R_{NRP} and R_{GPL} were used at 10 mg/mL and 4 mg/mL with 1 : 10 NADPH and 1 : 4 NADPH, respectively, with an exposure time of 1 h. Scattering was measured at 1.5418 Å with a 487 × 195 pixel Pilatus 100 K detector 300 mm from the sample. The scattering vector, $Q = 4\pi(\sin\theta)\lambda^{-1}$, where 2θ is the scattering angle and λ is the X-ray wavelength. The azimuthal averaging of raw data was done

using Fit2D2 program (11). The usable Q range of the azimuthally averaged data was limited to $0.02 < Q < 0.16$ Å^{-1}. The scattering data was analyzed and ab initio model generation was done using ATSAS (12) suite of programs. Radius of gyration was calculated using PRIMUS (13), the Dmax and $P(r)$ distance distribution were calculated using GNOM (14) and ab initio models were prepared using GASBOR (15).

1. Trivedi OA, et al. (2004) Enzymic activation and transfer of fatty acids as acyl-adenylates in mycobacteria. *Nature* 428:441–445.
2. Panjikar S, Parthasarathy V, Lamzin VS, Weiss MS, Tucker PA (2009) On the combination of molecular replacement and single-wavelength anomalous diffraction phasing for automated structure determination. *Acta Crystallogr D* 65:1089–1097.
3. Otwinowski Z (1997) Processing of X-ray diffraction data collected in oscillation mode. *Methods Enzymol.* 276:307–326.
4. Adams PD, et al. (2010) PHENIX: A comprehensive Python-based system for macromolecular structure solution. *Acta Crystallogr D* 66:213–221.
5. Jones TA, Zou JY, Cowan SW, Kjeldgaard M (1991) Improved methods for building protein models in electron density maps and the location of errors in these models. *Acta Crystallogr A* 47:110–119.
6. Emsley P, Cowtan K (2004) COOT: Model-building tools for molecular graphics. *Acta Crystallogr D* 60:2126–21232.
7. Brunger AT, et al. (1998) Crystallography & NMR system: a new software suite for macromolecular structure determination. *Acta Crystallogr D* 54:905–921.
8. Winn M, Isupov M, Murshudov GN (2000) Use of TLS parameters to model anisotropic displacements in macromolecular refinement. *Acta Cryst* 2001:D57 122–133.
9. Laskowski RA, MacArthur MW, Moss DS, Thornton JM (1993) PROCHECK—a program to check the stereochemical quality of protein structures. *J App Cryst* 26:283–291.
10. Sali A, Blundell TL (1993) Comparative protein modelling by satisfaction of spatial restraints. *J Mol Biol* 234:779–815.
11. Hammersley AP (1997) FIT2D: An Introduction and Overview. *ESRF Internal Report*, ESRF97HA02T.
12. Konarev PV, Petoukhov MV, Volkov VV, Svergun DI (2006) ATSAS 2.1, a program package for small-angle scattering data analysis. *J Appl Cryst* 39:277–286.
13. Konarev PV, Volkov VV, Sokolova AV, Koch MHJ, Svergun DI (2003) PRIMUS—a Windows-PC based system for small-angle scattering data analysis. *J Appl Crystallogr* 36:1277–1282.
14. Svergun DI (1992) Determination of the regularization parameter in indirect-transform methods using perceptual criteria. *J Appl Crystallogr* 25:495–503.
15. Svergun DI, Petoukhov MV, Koch MHJ (2001) Determination of domain structure of proteins from X-ray solution scattering. *Biophys J* 80:2946–2953.

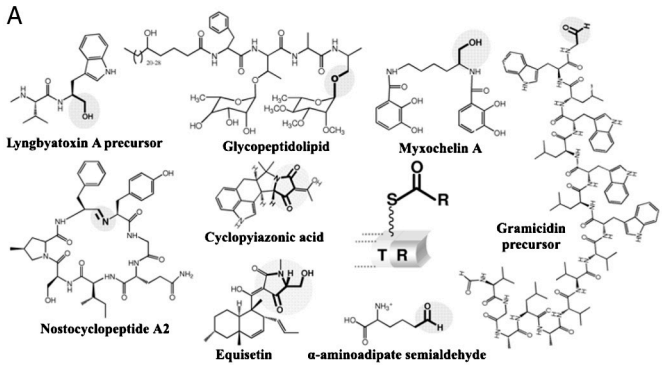

B

1	*M. tuberculosis H37 Rv*	15607243 (*Rv0101/nrp*)			
2	*M. smegmatis mc²*	118468008 (*MSMEG_0402/Mps2*)	118473501 (*MSMEG_2956*)	118467617 (*MSMEG_3715*)	118469671 (*MSMEG_5739*)
3	*M. bovis BCG*	121636014 (*BCG_0134*)	121638475 (*BCG_2613*)		
4	*M. leprae*	15827161 (*ML_0484*)			
5	*M. avium paratuberculosis*	41407340 (*MAP_1242*)	41407138 (*MAP_1040c*)	41409382 (*MAP_3284c*)	
6	*M. marinum*	183982131 (*MMAR_2117*)	183982939 (*MMAR_2936*)	183983944 (*MMAR_3972*)	

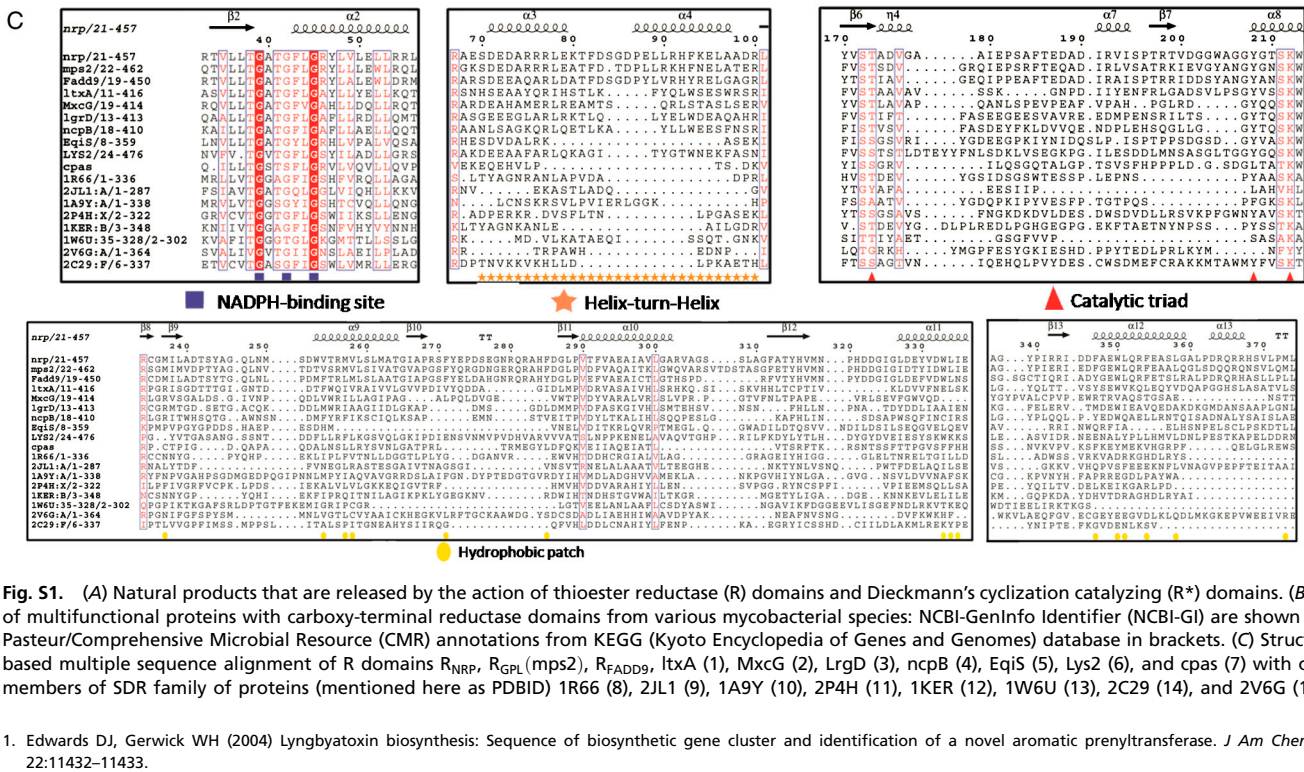

Fig. S1. (*A*) Natural products that are released by the action of thioester reductase (R) domains and Dieckmann's cyclization catalyzing (R*) domains. (*B*) List of multifunctional proteins with carboxy-terminal reductase domains from various mycobacterial species: NCBI-GenInfo Identifier (NCBI-GI) are shown with Pasteur/Comprehensive Microbial Resource (CMR) annotations from KEGG (Kyoto Encyclopedia of Genes and Genomes) database in brackets. (*C*) Structure-based multiple sequence alignment of R domains R_{NRP}, R_{GPL}(mps2), R_{FADD9}, ItxA (1), MxcG (2), LrgD (3), ncpB (4), EqiS (5), Lys2 (6), and cpas (7) with other members of SDR family of proteins (mentioned here as PDBID) 1R66 (8), 2JL1 (9), 1A9Y (10), 2P4H (11), 1KER (12), 1W6U (13), 2C29 (14), and 2V6G (15).

1. Edwards DJ, Gerwick WH (2004) Lyngbyatoxin biosynthesis: Sequence of biosynthetic gene cluster and identification of a novel aromatic prenyltransferase. *J Am Chem Soc* 22:11432–11433.
2. Silakowski B, et al. (2000) The myxochelin iron transport regulon of the myxobacterium StigmatellaaurantiacaSg a15. *Eur J Biochem* 267:6476–6485.
3. Kessler N, Schuhmann H, Morneweg S, Linne U, Marahiel MA (2004) The linear pentadecapeptide gramicidin is assembled by four multimodularnonribosomal peptide synthetases that comprise 16 modules with 56 catalytic domains. *J Biol Chem* 279:7413–7419.
4. Luesch H, et al. (2003) Biosynthesis of 4-methylproline in cyanobacteria: Cloning of nosE and nosF genes and biochemical characterization of the encoded dehydrogenase and reductase activities. *J Org Chem* 68:83–91.
5. Sims JW, Fillmore JP, Warner DD, Schmidt EW (2005) Equisetin biosynthesis in Fusariumheterosporum. *ChemCommun* 2:186–188.

6. Ehmann DE, Gehring AM, Walsh CT (1999) Lysine biosynthesis in Saccharomycescerevisiae: Mechanism of alpha-aminoadipatereductase (Lys2) involves posttranslational phosphopantetheinylation by Lys5. *Biochemistry* 38:6171–6177.
7. Liu X, Walsh CT (2009) Cyclopiazonic acid biosynthesis in Aspergillus sp.: Characterization of a reductase-like R* domain in cyclopiazonatesynthetase that forms and releases cycloacetoacetyl-L-tryptophan. *Biochemistry* 48:8746–8757.
8. Allard ST, Cleland WW, Holden HM (2004) High resolution X-ray structure of dTDPglucose 4,6-dehydratase from Streptomycesvenezuelae. *J Biol Chem* 279:2211–2220.
9. Kim MH, et al. (2008) Structural insight into bioremediation of triphenylmethane dyes by *Citrobacter* sp. Triphenylmethanereductase. *J Biol Chem* 283:31981–31990.
10. Thoden JB, Holden HM (1998) Dramatic differences in the binding of UDP-galactose and UDP-glucose to UDP-galactose 4-epimerase from *Escherichia coli*. *Biochemistry* 37:11469–11477.
11. Shao H, Dixon RA, Wang X (2007) Crystal structure of vestitonereductase from alfalfa (Medicago sativa L.). *J Mol Biol* 369:265–276.
12. Allard ST, et al. (2002) Toward a structural understanding of the dehydratase mechanism. *Structure* 1:81–92.
13. Alphey MS, Yu W, Byres E, Li D, Hunter WN (2005) Structure and reactivity of human mitochondrial 2,4-dienoyl-CoA reductase: enzyme-ligand interactions in a distinctive short-chain reductase active site. *J Biol Chem* 280:3068–3077.
14. Petit P, et al. (2007) Crystal structure of grape dihydroflavonol 4-reductase, a key enzyme in flavonoid biosynthesis. *J Mol Biol* 368:1345–1357.
15. Thorn A, et al. (2008) The crystal structure of progesterone 5beta-reductase from Digitalis lanata defines a novel class of short chain dehydrogenases/reductases. *J Biol Chem* 283:17260–17269.

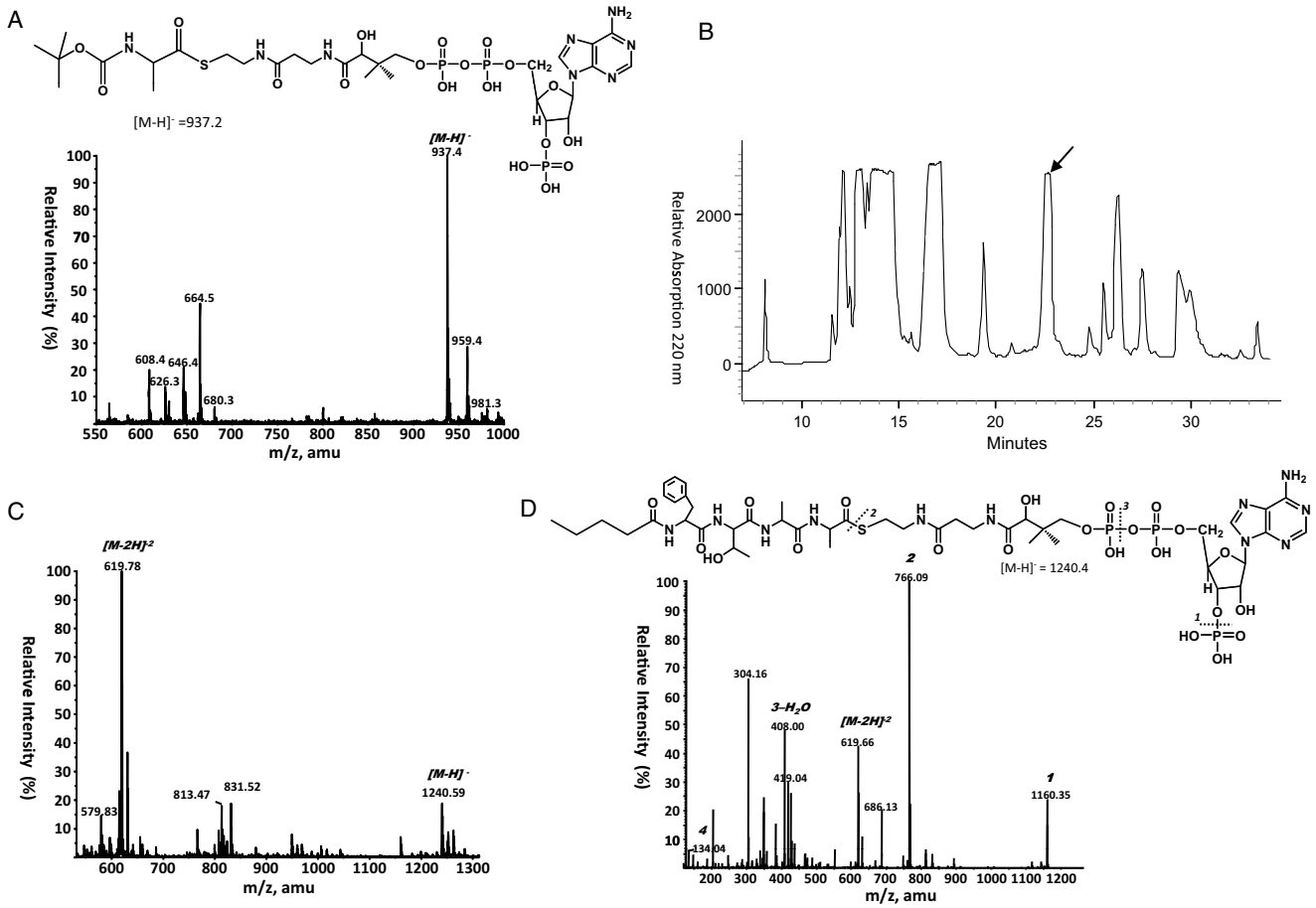

Fig. S2. Substrate analogs used for R_{GPL} analysis: (*A*) Mass spectrometric analysis of Boc-Alanyl-CoA m/z mass of $[M\text{-}H]^- = 937.2$. (*B*) HPLC purification of valeryl*D*-Phe-*D*-Thr-*D*-Ala-*L*-Alanyl coenzyme A. The peak at 22.5 min (marked with arrow) corresponds to valeryl-FTAA-CoA (*C*) Mass spectrometric analysis of valeryl-FTAA-CoA shows m/z mass of $[M\text{-}H]^- = 1240.6$ and doubly charged peak with m/z mass of $[M\text{-}2H]^{-2} = 619.7$. (*D*) Tandem mass spectrometric analysis and fragmentation pattern of doubly charged peak at $m/z = 619.7$.

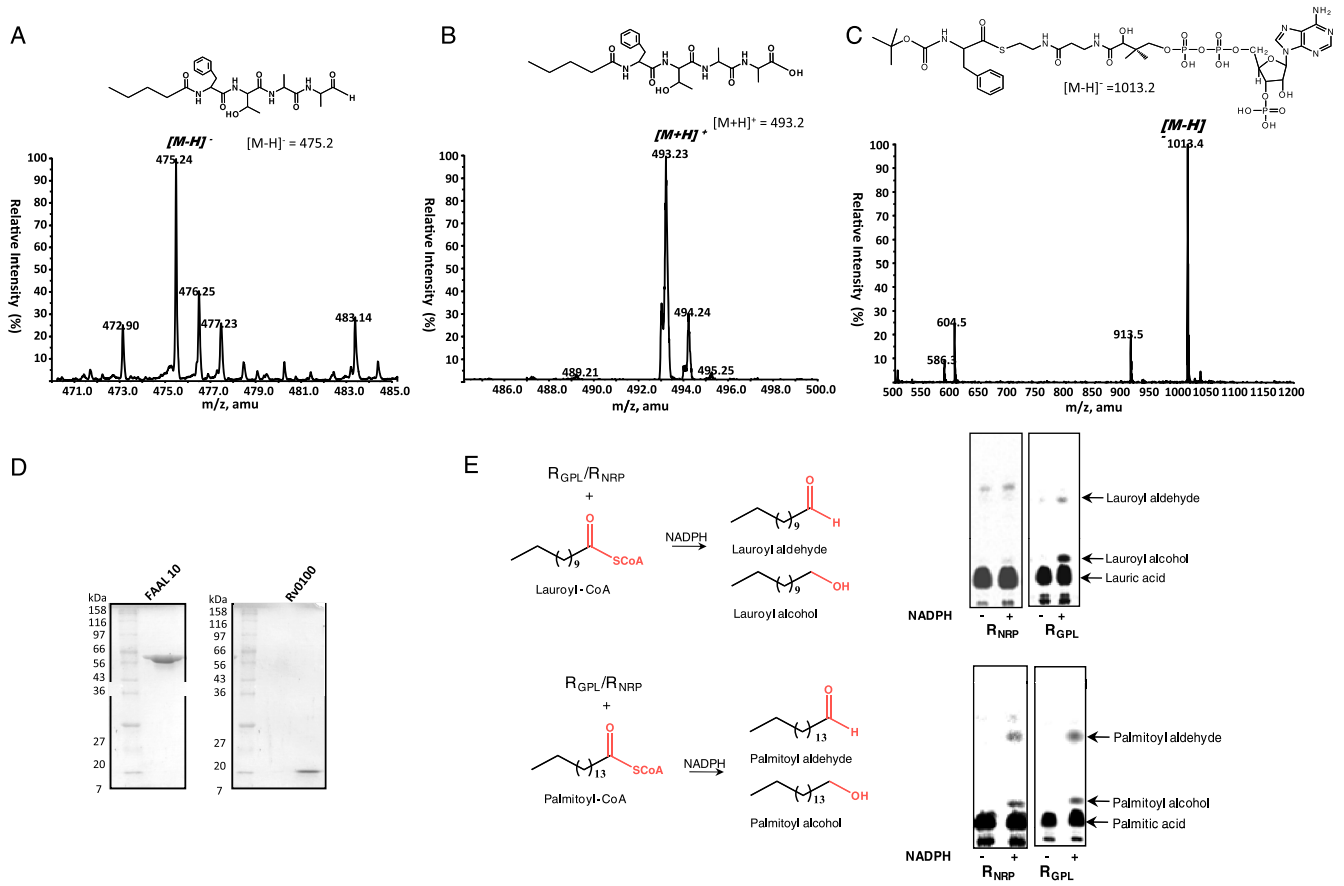

Fig. S3. Functional analysis of R_{GPL} and R_{NRP}: (*A*) Mass spectrometric analysis of peak I of Fig. 1*B* shows m/z mass of $[\text{M-H}]^- = 475.24$ corresponding to valeryl-FTA-Alaninal. (*B*) Mass spectrometric analysis of peak III of Fig. 1*B* shows m/z mass of $[\text{M} + \text{H}]^+ = 493.23$ corresponding to valeryl-FTA-Alanine. (*C*) Mass spectrometric analysis of Boc-Phenylalanyl-CoA m/z mass of $[\text{M-H}]^- = 1013.4$. (*D*) SDS-PAGE gel showing purified FAAL10 and Rv0100. (*E*) Radio-TLC analysis of R_{GPL} and R_{NRP} enzymatic assays with lauroyl-CoA and palmitoyl-CoA.

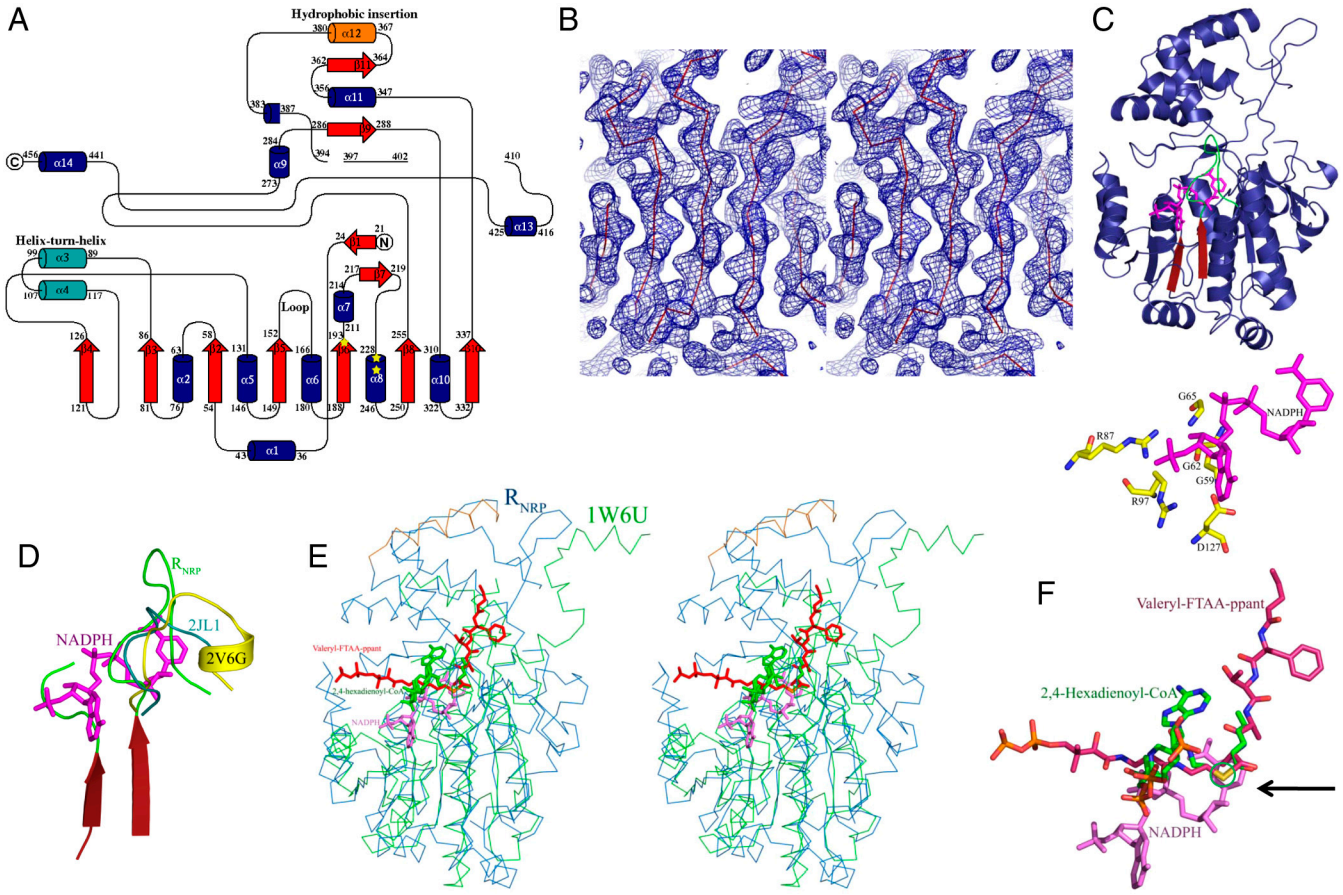

Fig. S4. R_{NRP} crystal structure: (*A*) The topology diagram of the R domain shows the helix-turn-helix (S90-D119) and loop (S153-F166) in the N-terminal domain and hydrophobic insertion (D366-L381) in the C-terminal domain. The catalytic residues T193, Y228, and K2323 are marked (as yellow asterisks). (*B*) An unbiasted SA-omit map. (*C*) NADPH modeled in R_{NRP} structure, shown here with the residues G59, G62, and G65 that constitute the GxxGxxG cofactor-binding motif and other conserved residues that interact with the cofactor. The NADPH is oriented based on superposition with other homologous structures. (*D*) In the R_{NRP} structure, which is solved in the absence of bound NAD(P)H, the loop S153 to F166 (red) occupies the region corresponding to the NADPH-binding pocket of 2jl1 (1) (green) and 2v6g (2) (violet). (*E*) The superimposed stereoimage of R_{NRP}, NADPH, and valeryl-FTAA-ppant (red) and 1W6U with its substrate 2,4-hexadienoyl-CoA (blue). (*F*) The sessile thioester bond is shown encircled and marked with an arrow with both valeryl-FTAA-ppant and 2,4-hexadienoyl-CoA superimposed.

1. Kim MH, et al. (2008) Structural insight into bioremediation of triphenylmethane dyes by *Citrobacter* sp. Triphenylmethanereductase. *J Biol Chem* 283:31981–31990.
2. Thorn A, et al. (2008) The crystal structure of progesterone 5beta-reductase from Digitalis lanata defines a novel class of short chain dehydrogenases/reductases. *J Biol Chem* 283:17260–17269.

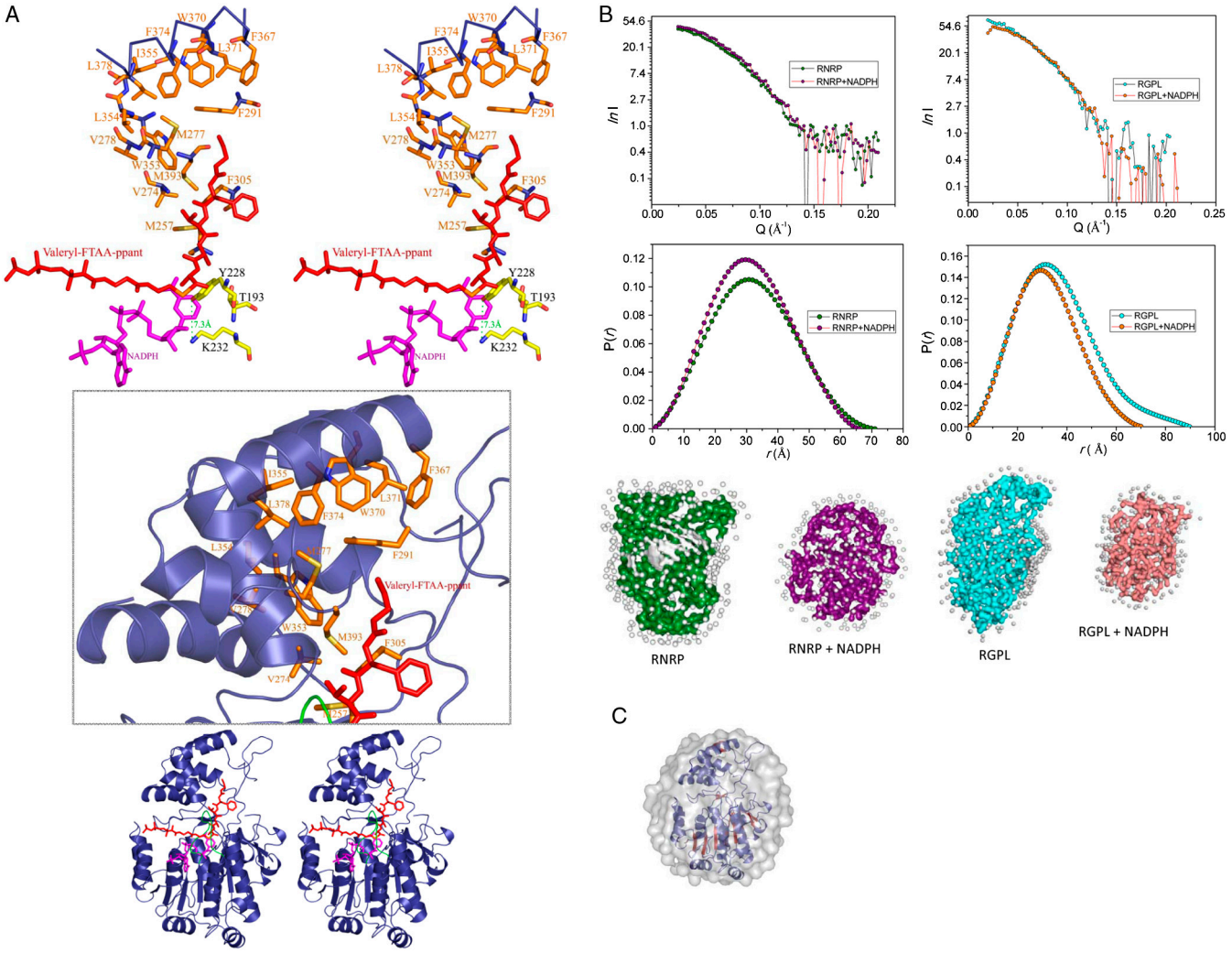

Fig. S5. (*A*) Conservation of residues putatively involved in catalysis and substrate binding, NADPH (magenta) and valeryl-FTAA-ppant (red) modeled in R_{NRP} structure. The catalytic residues Y228 and K232 and nicotinamide ring lie within catalytic distance of 2.1 Å and 7.3 Å, respectively, from the thioester bond (orange). Below it is the stereoview of the overall R_{NRP} (blue) with valeryl-FTAA-ppant (red), NADPH (magenta), and loop (green) and hydrophobic groove (orange). The valeryl chain extends into the C terminus and partially occupies a pocket surrounded by several hydrophobic residues which are conserved in R_{GPL} also (as shown in Fig. S1*B*). (*B*) SAXS intensity data and pair-distribution curves ($P(r)$) along with ab initio models. (*C*) The superimopsed crystal structure of R_{NRP} with SAXS envelope of R_{NRP} with NADPH suggests that the crystal structure represents the NADPH-bound or closed conformation.

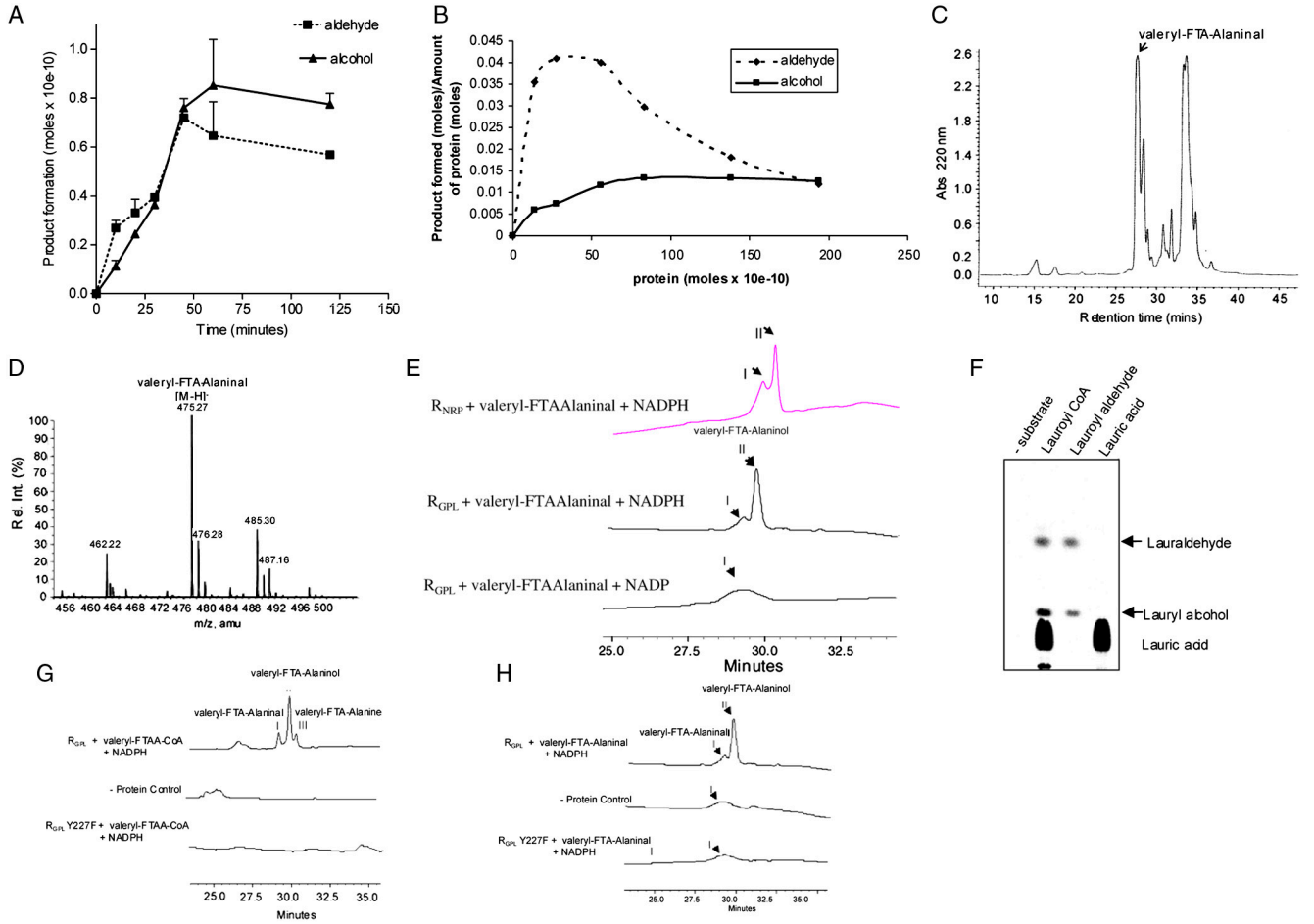

Fig. S6. (*A*) Time-dependent analysis of R_{GPL} reduction of lauroyl-CoA, plot of product formed (mean ± SD, $n = 2$) vs. time shows appearance of aldehyde first and increase in alcohol formation with time. (*B*) Effect of protein concentration on R_{GPL} product formation with lauroyl-CoA. (*C*) HPLC purification profile for valery-FTAAlaninal. The peak at 27 min corresponds to the aldehyde. (*D*) TOF-MS analysis of the 27 min peak shows molecular ion at m/z $[M\text{-}H]^- = 475.3$ corresponding to valeryl-FTAAlaninal. (*E*) HPLC analysis of R_{GPL} and R_{NRP} catalyzed reduction of valeryl-FTAAlaninal (I) shows valeryl-FTAAlaninol (II) formation, in the presence of NADPH. (*F*) Radio-TLC analysis of R_{GPL} assays shows lauroyl-CoA as well as lauroyl aldehyde reduction but no effect on lauric acid. Control reaction without substrate does not show any product formation. (*G*) HPLC analysis of WT R_{GPL} and Y227F R_{GPL} mutant enzyme assays with valeryl-FTAA-CoA substrate. The WT R_{GPL} protein reduces the thioester containing substrate analogue valeryl-FTAA-CoA, while the Y227F mutant protein is catalytically inactive. (*G*) The WT R_{GPL} protein reduces the lipopeptidyl aldehyde substrate valeryl-FTAAlaninal, while the Y227F mutant protein is catalytically inactive.

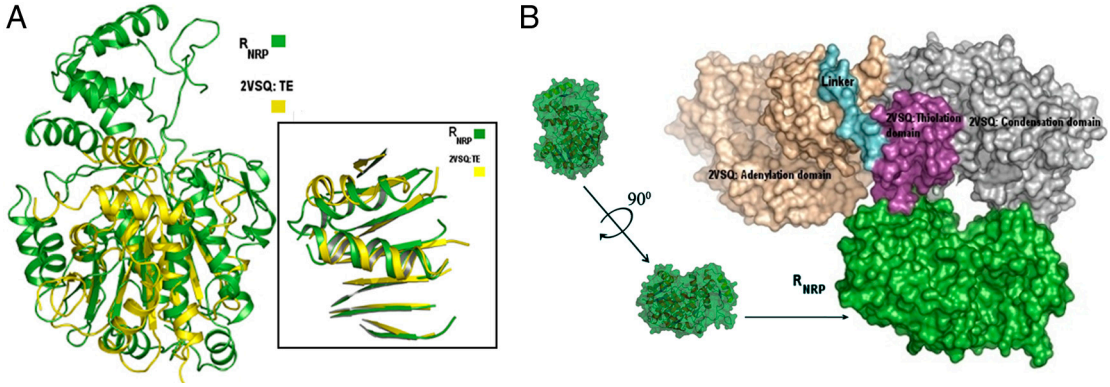

Fig. S7. Modeling of Nrp termination module: (*A*) Superimposition of the TE domain (yellow) of 2VSQ with R_{NRP} (green). (*Inset*) The similarity between the hydrolase fold and Rossmann fold is evident from the overlap of the central β sheet and the surrounding helices of the two domains. (*B*) Modeling of termination module of Nrp based on 2VSQ helped in replacing TE domain with R_{NRP} in the structure. Here the overall arrangement of R_{NRP} with respect to various domains of the termination module of 2VSQ is shown. The two R_{NRP} representations in *A* and *B* are related by 90°.

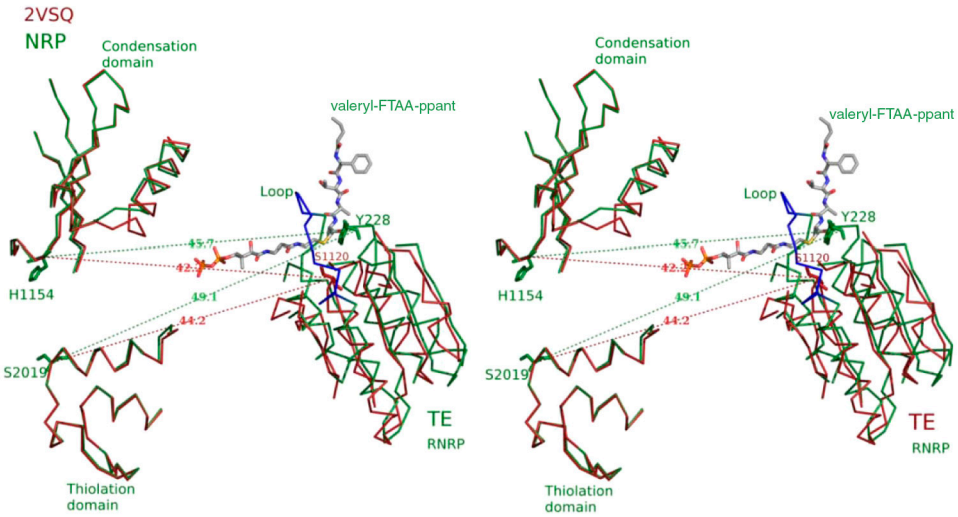

Fig. S8. The model of termination module of Nrp: Overlap of some regions of the modeled termination module of Nrp (green) with 2VSQ (1) (red) are shown along with the catalytic residues of various domains. The residues H1154, S2019, and Y2283 are the catalytic residues of C_2, T_2 and R_{NRP} domains of Nrp protein and S1120 is the catalytic residue of TE domain of 2VSQ. The distances between catalytic residues of various domains of Nrp are compared here with those published for 2VSQ. The loop S153-F166 is also shown here in blue.

1. Tanovic A, Samel SA, Essen LO, MarahielMA (2008) Crystal structure of the termination module of a nonribosomal peptide synthetase. *Science* 321:659–663.

Table S1. Data collection, phasing, and refinement statistics*

Data collection	R_{NRP}
Space group	$P3_121$
Cell dimensions	
a, b, c (Å)	59.06, 59.06, 239
α, β, γ (°)	90, 90, 120
Resolution (Å)	50-2.3 (2.38-2.3)
R_{sym}	0.092 (0.45)
$I/\sigma I$	25.05 (3.7)
Completeness (%)	99.9 (99.8)
Redundancy	12.10 (12.0)
Refinement	
Resolution (Å)	50.0-2.3
No. reflections	22,489
R_{work}/R_{free}	22.94/27.77
No. atoms	
Protein	3,285
Water	161
B-factors (Å^2)	
Protein	44.13
Water	49.64
rmsd	
Bond lengths (Å)	0.008
Bond angles (°)	1.111

*The data were collected from one crystal. Values in parentheses are for highest-resolution shell.

Table S2. List of primers used in the study

Protein	Primers used for amplification/mutagenesis of the gene sequence	
R_{GPL}	RSG 1806- tt cat atggccggt gag cgg acc gac	RSG 1807- ttgaattcagcagcccgagcagctgcag
R_{NRP}	RSG 1142- tt cat atggggcga gat gcccgaccg	RSG 1005- ttaagcttctacagcagtcc gag cag
T-R_{GPL}	RSG 1807- ttgaattcagcagcccgagcagctgcag	RSG 1062- tt cat atgctcgccggcatcttcgcc
T-R_{NRP}	RSG 1061- tt cat atg gag aag acc gtggccggc	RSG 1005- ttaagcttctacagcagtcc gag cag
FAAL10	RSG 248- cat atgggaggaaagaagtttcaa	RSG 250- ctc gag tcagccacgaacgaccactctggc
Rv0100	RSG-999- tt cat atgcgggaccgaatcctcgcc	RSG 1001- aagaattcccgaactcggtgcacac a
R_{GPL} Y227F	RSG 2501- gccaacggcttcgggaattccaagtgggcaggc g	RSG 2502- c gcctgcccacttggaattcccgaagccgttggc
R_{GPL} T192A	RSG 2564- c aacttcgtgtcggcgtcggacgtcggc	RSG 2565- Gccgacgtccgacgccgacacgaagtt g
R_{GPL} K231A	RSG 2613- c gcc aac ggc tac ggg aat tcc gcg tgg gca ggc gag g	RSG 2614- c ctc gcc tgc cca cgc gga att ccc gta gcc gtt ggc g